Some Comparisons of Turboramjet-Powered Hypersonic Aircraft for Cruise and Boost Missions

RICHARD H. PETERSEN,* THOMAS J. GREGORY,* AND CYNTHIA L. SMITH†
NASA Headquarters, Moffett Field, Calif.

The results of a launch-vehicle mission analysis are presented and compared with those of a previous analysis of hypersonic transport missions. The launch vehicles studied consist of hypersonic aircraft first stages, which are powered by hydrogen-fueled, subsonic-burning turboramjets, and H_2-O_2 rocket second stages. A parametric investigation of the vehicle characteristics and the trajectory is presented and used to indicate the maximum payload capability of the launch systems. First-stage parameters that were varied include wing loading, fuselage slenderness ratio, wing thickness, and aspect ratio. Trajectory parameters that were varied include lateral-range requirement, cruise Mach number, and turn radius. Parameters examined that affect the staging maneuver include maximum normal acceleration, maximum allowable angle of attack, and dynamic pressure at staging. The parametric tradeoffs reflect the variations in fuel consumption caused by aerodynamic and propulsive efficiency changes and the variations in structural weight because of environmental heating and structural loading changes. The results indicate that launch vehicles are characterized by lower fuselage volumes and higher wing loadings than those associated with a hypersonic transport, but only small penalties result from using transport-like characteristics for the launch vehicles. Although the launch vehicle geometries and trajectories differ from those of a transport, the technology requirements are found to be similar.

Introduction

RECENT mission studies[1-3] have indicated that hydrogen-fueled, air-breathing, hypersonic aircraft have attractive performance capabilities for both cruise and boost missions. For cruise missions such aircraft offer promise of carrying sizable payloads over large ranges at high speed. When used as the first stage of an orbital launch system they are potentially capable of placing manned payloads in Earth orbit, inherently reusable, can operate from existing airfields, and can be designed to launch into orbital planes at a considerable distance from their base. Although the cost of developing either a cruise or a launch vehicle would be high, it is possible that a large portion of the cost might be equally applicable to either type of vehicle. In this event, both a cruise vehicle and a launch vehicle could be developed for only a slightly greater cost, and the development costs could be spread over many more aircraft and missions. In order to assess these possibilities, it is necessary to investigate the performance capabilities of both cruise and launch aircraft and to determine to what extent the vehicles and their associated technology requirements are similar.

In a previous paper[3] the results of a parametric study of the performance of hypersonic cruise aircraft were reported. The purpose of the current paper is to present the results of a similar study of hypersonic, airbreathing, launch vehicles and to compare these results with those obtained for the cruise mission. The following discussions refer primarily to the performance and design tradeoffs associated with launch vehicles. These tradeoffs are analyzed in order to obtain preliminary estimates of the performance and other characteristics of near-optimum vehicles. Where appropriate, references will be made to the results of the earlier cruise-vehicle study. The methods and approaches used in the launch-vehicle analysis will be discussed first; then the results of the tradeoff studies will be presented.

Presented as Preprint 65-759 at the AIAA/RAeS/JSASS Aircraft Design and Technology Meeting, November 15–18, 1965, Los Angeles, Calif.; submitted December 10, 1965; revision received Apil 29, 1966.

* Research Scientist, Office of Advanced Research and Technology, Mission Analysis Division. Member AIAA.

† Mathematician, Office of Advanced Research and Technology, Mission Analysis Division.

Methods

A preliminary mission analysis of launch vehicles involves determining the values of vehicle parameters that yield maximum payload in orbit. Most parameters influence both the inert weight and the fuel weight of the vehicles, usually with opposing effects on the payload. To determine these effects, the present analysis utilized a mathematical-model technique in which computations of structural weight, aerodynamic performance, and propulsion-system performance were based on vehicle geometry, sizing, and trajectory parameters. These computations were performed on a digital computer in conjunction with trajectory computations. The integrated computations simulated the flight of both stages of the vehicle and properly related the separate problems of structural weight and fuel consumption.

Analysis Model

The first-stage vehicles chosen for analysis had large volume fuselages, triangular wings, and suitable tail surfaces. A typical configuration is shown in Fig. 1. The aerodynamic lift and drag of each configuration were estimated[4-8] from its geometry and flight Mach number; the estimates of friction drag included the effects of the trajectory on Reynolds number. The structural weights and thermal-protection weights were estimated[9,10] from the vehicle geometry, imposed loads, and temperature environment. The airframe skin and leading edges were considered to be cooled by radiation, but regenerative cooling was considered for the internal surfaces of the propulsion system. The propulsion-system inlet was placed in the wing compression field and was a variable-geometry, mixed-compression type. The pressure recovery was estimated but also was varied as a parameter. The engines were hydrogen-fueled, subsonic-burning turboramjets. The engine and exhaust-nozzle performance and weight were derived from manufacturers' estimated data. The exhaust-nozzle flow was assumed to be in equilibrium.[11]

As indicated in Fig. 1, the second stage was considered to be carried internally. It was assumed to be an expendable ballistic rocket, powered by a liquid-oxygen—liquid-hydrogen rocket engine. The orbital payload was considered to be carried in the nose of the second stage.

Mission Trajectories

The nominal climb trajectory used in the present study is shown in Fig. 2. It consists of a typical subsonic climb, followed at higher speeds by a climb along a 3 psf sonic-boom overpressure line[12,13] to about Mach number 3, and then a climb at a dynamic pressure of 2000 psf. This trajectory is consistent with the nominal one that was used in the cruise-vehicle study.[3] While the sonic-boom limit is somewhat high, it is based on far-field effects. Recent research on near-field effects[14] indicates that properly designed aircraft may be able to fly trajectories such as the one shown in Fig. 2 with greatly reduced sonic overpressures. Furthermore, launch vehicles probably would be operated from more isolated areas and much less frequently than transport aircraft.

Three typical ground paths for the boost mission are shown in Fig. 3. Since airbreathing aircraft are suited well to cruising in the atmosphere before launching their second stage, they can be used to launch payloads into orbital planes at some distance from their base. To investigate this capability, one of the vehicles in the following study was required to have a lateral range capability of 2000 naut miles (lateral range is defined as the perpendicular distance from the takeoff point of the aircraft to the launch plane of the second stage), and its performance was investigated for lateral ranges from 0 to 2000 nautical miles. Since a requirement for lateral range influences the vehicle configuration, a second vehicle with no lateral range requirement also was studied. In all cases, the first stage was considered to return to its takeoff site by cruising at its design Mach number and making a maximum L/D descent. At the shorter lateral ranges this type of return flight may not be optimum, but it does give an indication of performance potential. The ground paths shown in Fig. 3 are drawn to scale for 1.5 g turns at a design Mach number of 7.

Second-Stage Launch Maneuver

If the second stage is launched from the first stage in level flight, the high dynamic pressure can cause separation problems and the second stage will suffer high drag losses before it climbs out of the sensible atmosphere. To avoid these difficulties, it was assumed that the first stage would perform a pull-up maneuver before launching the second stage. For the second stage, the ascent trajectory involved two periods of burning for the rocket engine. The first burn established a Hohmann transfer ellipse, and the second burn injected the entire second stage into a circular orbit at 262 naut miles. A steepest-ascent computer program[15,16] was used to optimize the angle-of-attack schedule during the first burn; the second burn was assumed to be impulsive.

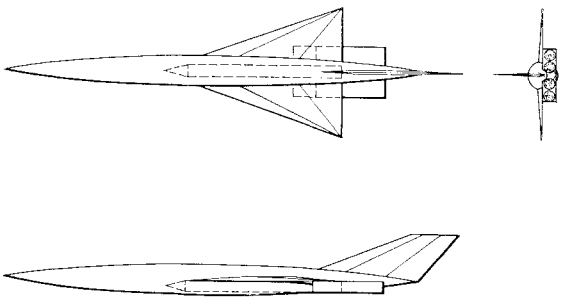

Fig. 1 Typical configuration.

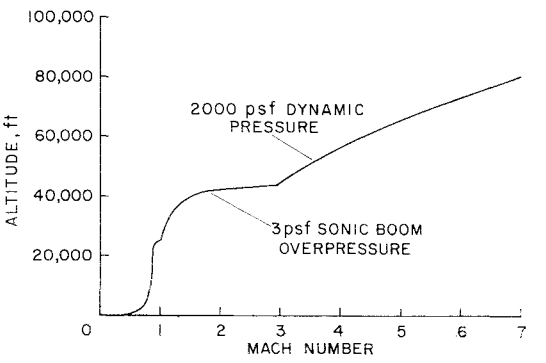

Fig. 2 Nominal climb trajectory.

Tradeoff Results

The results of the launch-vehicle tradeoff studies will cover some of the effects of thrust loading, inlet performance, fuselage fineness ratio, wing loading, aspect ratio, wing thickness ratio, first-stage turn radius, second-stage launch maneuver, design Mach number, and lateral range. In most cases, the results will be presented in terms of fractions of the vehicle gross takeoff weight, with the objective being to obtain a maximum fraction for the second-stage launch weight. The payload in orbit generally is not shown because the ratio of payload weight to second-stage launch weight is usually constant; when this ratio is not constant, the payload fraction in orbit will be indicated. Results usually are presented for a vehicle designed for 2000-naut-miles lateral range and for one designed for zero range. In this way the influence of the lateral-range requirement will be evaluated.

The nominal vehicles for the tradeoff studies had a gross takeoff weight of 500,000 lb and a design Mach number of 7. They had a fuselage fineness ratio of 14, a takeoff wing loading of 80 psf, and a takeoff thrust loading of 0.50. The wing aspect ratio and thickness ratio were 1.45 (leading-edge sweep of 70°) and 0.04, respectively. The 2000-naut-mile vehicle had a fuselage volume of 56,600 ft^3, while the fuselage volume of the zero-range vehicle was 42,000 ft^3.

Engine

The results of the tradeoff in turbojet size are shown in Fig. 4. The thrust loading, i.e., the ratio of takeoff thrust to gross takeoff weight, was used as a measure of turbojet size. The propulsion-system weight, of course, increased with increasing turbojet size; but the fuel consumption decreased because of the shorter times involved in accelerating, particularly through the transonic speed regime. The airframe weights decreased slightly at the higher thrust-to-weight ratios because of the reduction in fuel-tank size. The second-

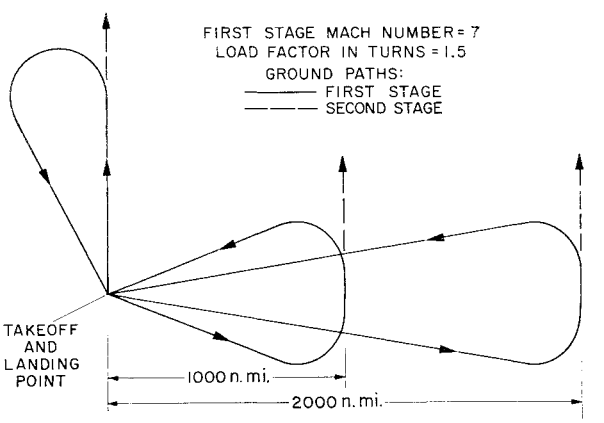

Fig. 3 First-stage ground paths.

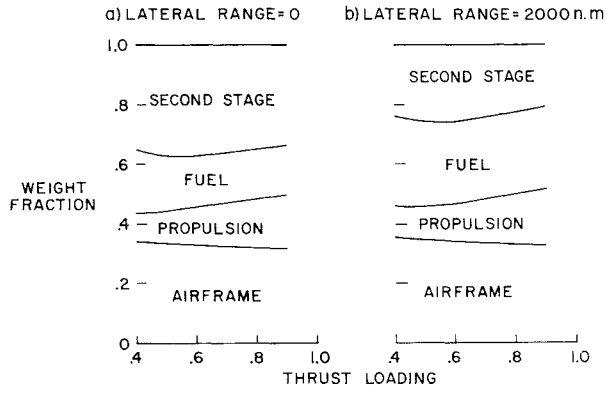

Fig. 4 Effect of thrust loading.

stage launch weight was maximum for a thrust loading of 0.55 for both the 2000-mile vehicle and the zero-range vehicle. This value compares to an optimum thrust loading of 0.45 for the cruise vehicles studied earlier.[3] However, in all cases the curves in Fig. 4 are quite flat, and a thrust loading of 0.50 was used as nominal in the present study.

For the present study, the ramjet was operated at stoichiometric fuel-air ratio and was sized so that the aircraft would cruise near $(L/D)_{max}$. Parametric variations of both fuel-air ratio and ramjet size indicated that these conditions gave near optimum performance for both the 2000-mile vehicle and the zero-range vehicle (and also for the cruise vehicle[3]).

Dynamic Pressure

Although the nominal climb path was limited to a dynamic pressure of 2000 psf, several climb paths with different dynamic pressure limitations also were investigated. As indicated in Fig. 5, the airframe weight was relatively insensitive to dynamic pressure limits. The present study did not consider aeroelastic effects which are difficult to estimate without detailed structural models. However, aeroelastic problems normally can be solved by good structural design without incurring weight penalties, and therefore, the trend shown in Fig. 5 probably is valid. Since the internal pressure in the inlet and engine was limited to 200 psi, the propulsion-system weight also did not vary with changes in the dynamic pressure limits. For the zero-range vehicle, the greater time and distance required to climb along a lower dynamic pressure trajectory resulted in greater fuel consumption both before the launch and on the return flight. Thus, a high dynamic pressure limit appears favorable for the zero-range vehicle. For the 2000-naut-mile mission, the additional time to climb did not result in severe performance penalties because the latter portion of climbing flight is almost as efficient as cruise flight. The results for the 2000-naut-mile mission are similar to those obtained in the cruise vehicle studies[3]; the performance is relatively constant for dynamic pressures between 1000 and 2500 psf. If the 2000-naut-mile vehicle also would be required to perform zero-range missions, it probably is preferable to design it for a dynamic pressure of 2000 or 2500 psf so that it could perform both short and long range missions efficiently.

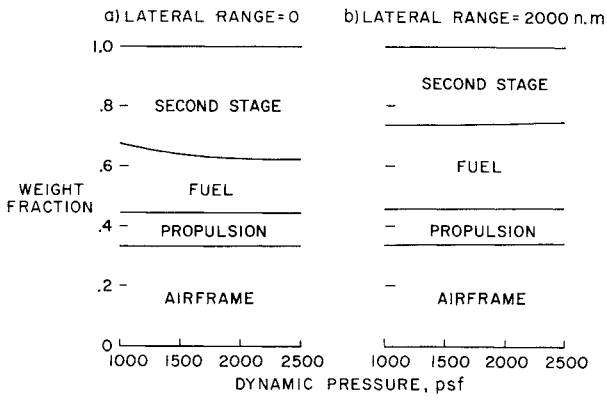

Fig. 5 Effect of dynamic pressure during climb.

Inlet

The standard pressure-recovery schedule used in this study is shown in Fig. 6a. It is derived from a schedule suggested by the military (MIL-E-5008B).[17] The military schedule is referenced to freestream conditions, but in the present study it was desired to consider the effects of wing angle of attack. For this purpose, the military schedule was considered to correspond to a wing angle of attack of 6°. With this assumption, the schedule shown in Fig. 6a, which is based on conditions in the flowfield just ahead of the inlet, was obtained. When this schedule is used with a trajectory having a dynamic pressure of 2000 psf, the internal pressure in the propulsion system reaches a maximum of 400 psi, which results in a relatively heavy inlet and engine. An investigation was made to determine if the over-all performance was improved by reducing the pressure recovery sufficiently to restrict the internal pressure to a given value. Figure 6b shows the tradeoff with maximum allowable internal pressure, whereas the dotted lines in Fig. 6a indicate the recovery schedules associated with each value of the internal pressure. (Note that as the airplane approaches its maximum Mach number and climbs to cruise altitude, the recovery schedules double back because of changes in the ambient pressure and in the wing compression field Mach number.) As expected, the propulsion-system weight decreases as the allowable internal pressure is decreased and the fuel consumption increases because of the reduced pressure recovery. The second-stage curve indicates a relatively flat optimum for internal pressure limits of 150 to 200 psi. The results shown are for launch vehicles with a 2000-mile lateral range, but similar results were obtained in the present study for the zero-range vehicle and previously for cruise vehicles.[3] In all three cases a nominal internal pressure limit of 200 psi was chosen.

It also is interesting to investigate what would happen if the standard pressure-recovery schedule could not be achieved. In Fig. 7a, the standard schedule is shown again along with several schedules which are identical up to Mach number 3, but the pressure recovery then is reduced to various percentages of the standard recovery at an inlet Mach number of 6. The percentage reduction was assumed to vary linearly with Mach number. The line representing a 200-psi internal pressure limit also is shown because the pressure recovery was not allowed to exceed the recovery that gave a pressure of 200 psi. The mission performance with the reduced pressure-

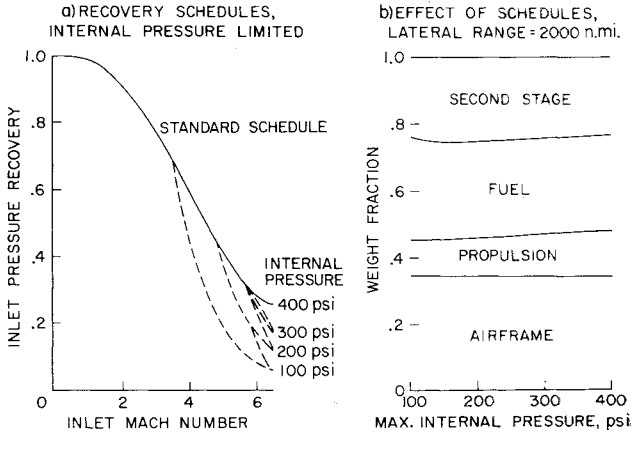

Fig. 6 Effects of limiting internal pressure.

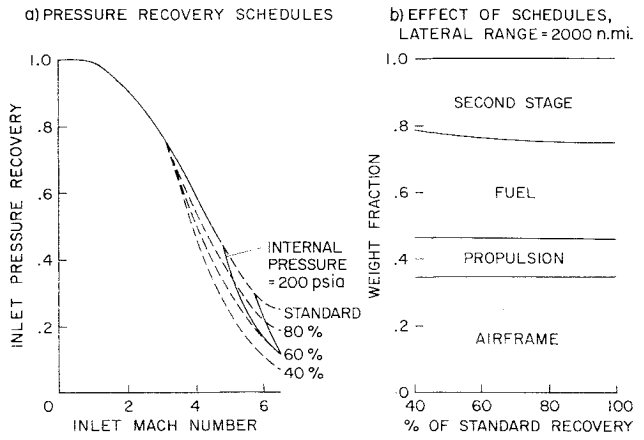

Fig. 7 Effect of inlet pressure recovery.

recovery schedules is presented in Fig. 7b. The airframe and propulsion weights are insensitive to changes in pressure-recovery schedule, but the fuel weight increases as the recovery is reduced with resulting losses in second-stage weight. However, the losses are not severe for a pressure recovery of 80% of nominal, which indicates that the mission performance is not sensitive to small reductions in pressure recovery. This conclusion also was found to be valid for the zero-range vehicle and the cruise vehicle.[3]

Fuselage

Results of the tradeoffs related to fuselage fineness ratio are shown in Fig. 8. As the fuselage length increases, its weight increases as indicated by the dotted line. The curve of total airframe weight has a slightly different shape because of differences in fuel tank sizes, but the trend of increasing weight is nearly the same. Both the propulsion-system weight and the fuel weight decrease with increasing fineness ratio because of the reduction in drag. The resulting second-stage weight is maximum at a fineness ratio of about 14, the nominal value used in the present study. This value corresponds to a length of 288 ft for the 2000-naut-mile vehicle, which has a fuselage volume of 56,600 ft^3; the zero-range vehicle has a length of 261 ft and a volume of 42,000 ft^3. Although the cruise vehicle also carried a maximum payload for a fineness ratio of about 14, a nominal value of 12 was used in the cruise study[3] to reduce the fuselage length. The nominal cruise vehicle had a length of 285 ft and a volume of 71,500 ft^3.

Wing

The effect of changes in takeoff wing loading is indicated in Fig. 9. As shown by the dotted line, the wing weight decreases as wing size decreases. The weights of the remainder

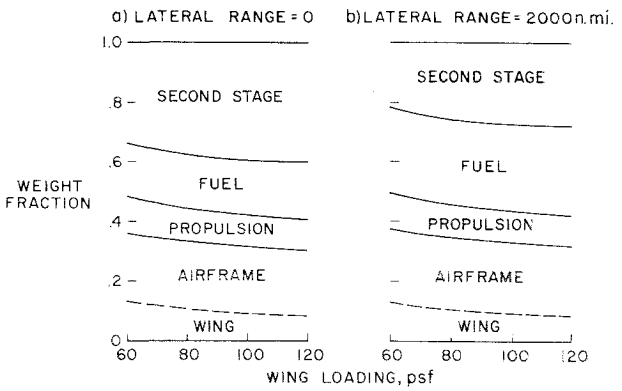

Fig. 9 Effect of wing loading.

of the airframe and of the propulsion system are almost unaffected by the change in wing loading. A slight increase in fuel weight with increased wing loading results from the reduction in lift-drag ratio due to the smaller wing. The maximum second-stage weight was achieved at a wing loading of about 120 psf, but it will be shown, subsequently, that this wing loading is probably too high for landing and takeoff. Thus, a nominal wing loading of 80 psf, which corresponds to the optimum value obtained in the cruise-vehicle study,[3] also was used in the present study, although it resulted in some degradation of performance.

The wing aspect ratio tradeoff shown in Fig. 10 indicates that the small reduction in wing weight with lower aspect ratio results in a corresponding small increase in second-stage weight. Again, such a trend may not be usable since lower aspect ratios make the landing and takeoff problem more severe. In fact, the shallow slope of the curves in Fig. 10 suggests that aspect ratios higher than 1.45, the nominal for this study, might give improved low-speed performance with only slight payload penalties. Essentially, the same conclusions were true for cruise vehicles.[3]

The results in Fig. 11 give an indication of the landing problem. The angle of attack necessary for a touchdown speed of 175 knots is shown as a function of the aspect ratio and takeoff wing loading. (For these results, the ground effect is neglected, and it is assumed that the second-stage oxidizer would be jettisoned in an emergency resulting in a maximum landing weight of about 80% of the gross takeoff weight.) For the nominal study vehicle with an aspect ratio of 1.45 and a takeoff wing loading of 80 psf, an angle of attack of about 16° is required. Of course, normal landings will be at lower weights so that the angle and/or the speed could be reduced somewhat. It is obvious, however, that landing and takeoff requirements will have a strong influence on the design of both cruise and launch vehicles.

The effect of changes in the wing thickness ratio is shown in Fig. 12. The primary change in airframe weight resulted

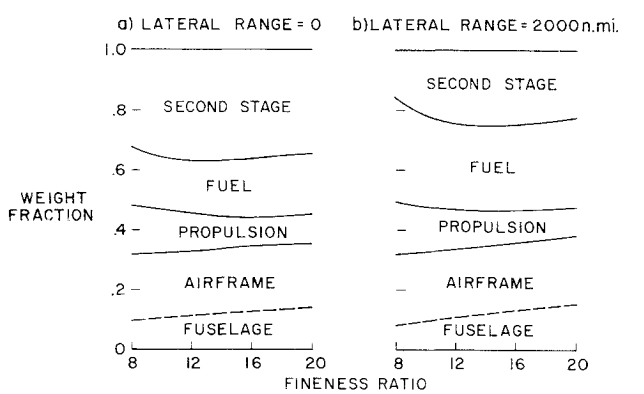

Fig. 8 Effect of fuselage fineness ratio.

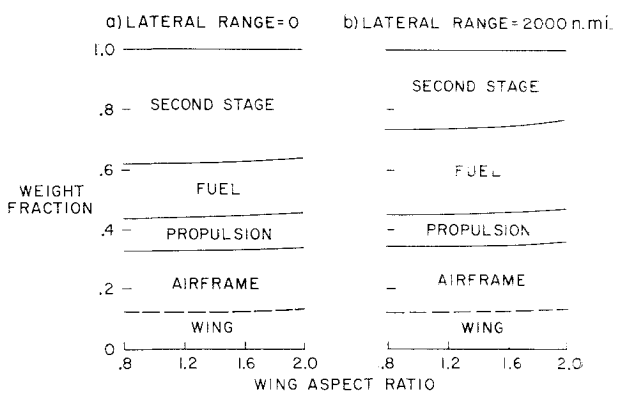

Fig. 10 Effect of wing aspect ratio.

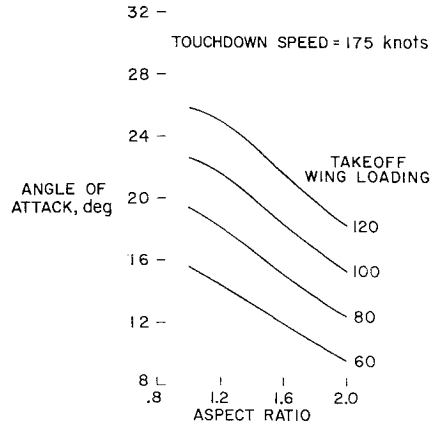

Fig. 11 Angle of attack for landing.

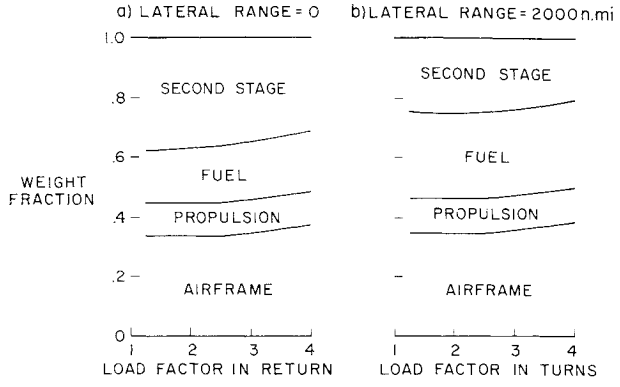

Fig. 13 Effect of load factor in turns.

from the change in wing weight, which decreased as the wing thickness increased. However, the thicker wings created higher drag with attendant increases in propulsion and fuel weight. As a result, the second-stage weight peaked near a thickness ratio of 0.04, the nominal value used in this study. The cruise-vehicle study[3] showed the same result, an optimum thickness ratio of 0.04.

Ground Path

The ground paths shown in Fig. 3 were obtained with 1.5 g turns at a Mach number of 7. It is interesting to examine various turn radii since tighter turns decrease the path length but increase drag and sometimes design structural loads. The resulting effects on weight are shown in Fig. 13 as a function of the normal load factor in the turn. Both the airframe weight and the propulsion system weight are constant up to a load factor of 2.5, which is the design load factor assumed for cruise flight. Above this load factor, the airframe weight increases because the design load factor must be increased. The fuel weight fraction increases very slowly as the load factor is increased from 1.25, indicating that the increase fuel consumption in the high-g turns more than compensates for the decrease in fuel consumption due to shorter flight paths. It appears then that the requirement for high-speed turns will not have a significant effect on the design of the launch vehicle since these turns can be performed at relatively low load factors.

Launch Maneuver and Second-Stage Trajectory

As was indicated previously, the airbreathing first stage was considered to perform a pull-up maneuver before launching the second stage. This maneuver has two advantages; it results in improved performance by reducing second-stage drag and gravity losses; and it reduces the dynamic pressure at launch, which eases the problems associated with separating the two stages. A typical launch maneuver and second-stage trajectory are shown in Figs. 14 and 15. The first stage started from the Mach 7 cruise condition and pulled up with a normal load factor of 1.5. Second-stage launches were assumed from successive points along the first-stage trajectory, and it was determined that the launch point shown in the figures gave maximum payload in orbit. The angle-of-attack time history for the second stage was determined with a steepest-ascent optimization program. (The slight increase in dynamic pressure shown in Fig. 15 at the end of the trajectory can be eliminated with no loss in payload by slightly modifying the angle-of-attack history.) The figure shows the trajectory only for the first burn of the second stage; the second stage then coasts halfway around the earth and makes a short second burn to achieve a circular orbit at 262 naut miles. For the conditions shown in Figs. 14 and 15, the velocity increment in the second burn is 394 fps.

With a given aircraft and an initial set of flight conditions, the first-stage pull-up was considered to be controlled by first holding a constant normal load factor until a specified angle of attack was reached and then holding that maximum angle of attack constant. The effects of varying the pull-up load factor and the maximum angle of attack are shown in Fig. 16. Maximum performance in terms of the payload in earth orbit was obtained for a pull-up load factor of 2.5, but the payload degradation associated with a 1.5 g pull-up was only 0.5%. Since the lower load factor pull-up eases the structural and thermal problems of the first stage and also results in a lower dynamic pressure at launch, a load factor of 1.5 and an angle-of-attack limit of 15° were used to define the nominal pull-up.

The effects on the payload delivered to orbit of the dynamic pressure at the start of the pull-up and at launch are shown in Fig. 17. For the nominal configuration, the dynamic pressure during the cruise portion of flight is 834 psf. The design dynamic pressure for this configuration is 2000 psf. It was thought that better performance might be obtained if the

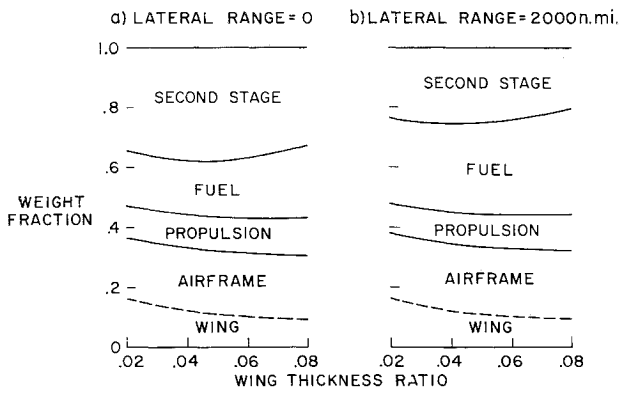

Fig. 12 Effect of wing thickness ratio.

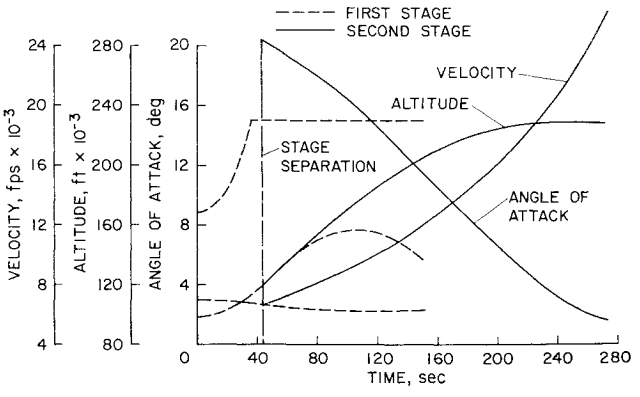

Fig. 14 Nominal launch maneuver.

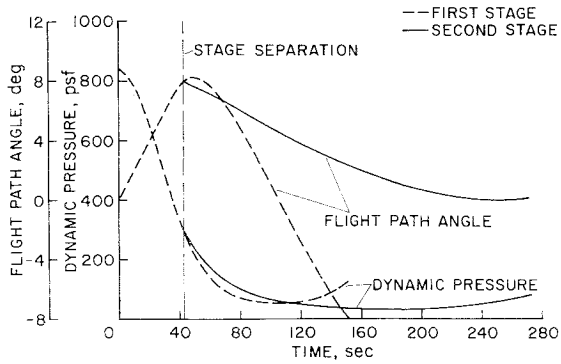

Fig. 15 Nominal launch maneuver.

pull-up were initiated at a lower altitude corresponding to the higher dynamic pressure. As indicated in the figure, this proved to be the case, but the improvement in the payload was less than 0.5%; and the dynamic pressure at launch was 400 psf as compared to 300 psf when the pull-up was initiated from the cruise altitude. For these reasons, the pull-up from the cruise altitude was considered as the nominal case. The results in Fig. 17 also show the penalty associated with reducing further the launch dynamic pressure; a reduction from 300 to 100 psf can be obtained with a payload reduction of 3%. Thus, if stage separation proves to be a severe problem, some of the difficulty could be reduced by launching somewhat later in the first-stage pull-up and accepting some loss in payload.

It appears then that neither the high-speed turns nor the pull-up maneuver associated with the launch missions result in unusual load-factor design requirements for the first stage. In fact, the nominal cruise vehicle from the previous study,[3] which had a design load factor of 2.5, is fully capable, in this regard, of the required turn and pull-up maneuvers.

The performance tradeoff with second-stage initial thrust loading is shown in Fig. 18. Although the propellant weight decreased slightly at higher thrust loadings, the rocket engine weight increased; consequently, the maximum payload was obtained for initial thrust loadings of 1.5 or slightly less. In drawing the curves of Fig. 18, it was assumed that the second-stage structural weight was constant. In fact, this weight probably would increase at the higher thrust loadings causing further reductions in the payload. The propulsion weight in the figure is based on a rocket engine thrust-to-weight ratio of 70, but even assuming a more optimistic ratio of 100 does not change the optimum significantly. Therefore, an initial thrust loading of 1.5 was used in the present study.

With an initial thrust loading of 1.5 and a constant thrust engine, the maximum acceleration of the second stage is almost 8 g. If the rocket engine can be throttled to about 40% of full thrust, it is possible to limit the second-stage acceleration to 3 g. Such a limit is desirable for manned

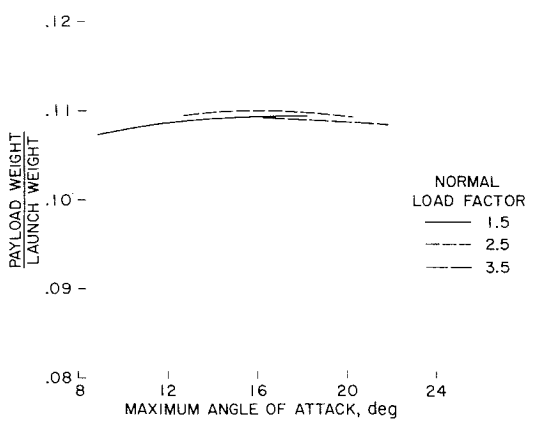

Fig. 16 Effect of first-stage pull-up on second-stage performance.

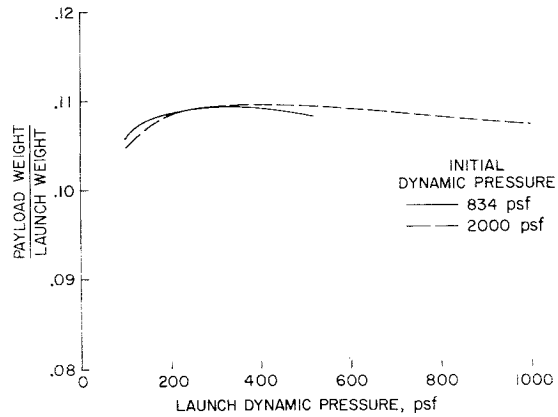

Fig. 17 Effect of launch dynamic pressure on second-stage performance.

vehicles, although not necessary. It was found that for optimized second-stage trajectories with thrust histories limiting the acceleration to 3 g, the increase in propellant weight amounted to only 0.5% of the payload weight. Therefore, if the throttleable engine does not weigh considerably more than a fixed-thrust engine, the second-stage acceleration can be limited to 3 g with only a small penalty in payload capability.

Design Mach Number

The effect of varying the first-stage design Mach number in the range from 4 to 7 is shown in Fig. 19. As expected, the airframe, propulsion, and fuel weights increased with increasing Mach number resulting in reductions in the second-stage launch weights. Of course, at the lower launch velocities the second stage must provide a higher velocity increment. The resulting payload curve at the top of Fig. 19 indicates a rather flat maximum in the region between Mach numbers 6 and 7, with poorer performance at lower speeds. Speeds above Mach number 7 were not considered in the present study because of the engine cooling problems associated with subsonic-burning ramjets at higher speeds. Although the payload in orbit was slightly better at Mach number 7, a launch vehicle operating at Mach number 6 might be of special interest because the previous study[3] of cruise vehicles showed best payload performance at this speed. With this choice, the technology requirements for both vehicles would be virtually identical.

Lateral Range

The orbital payload capability of the various vehicles studied is presented in Fig. 20 as a function of the mission

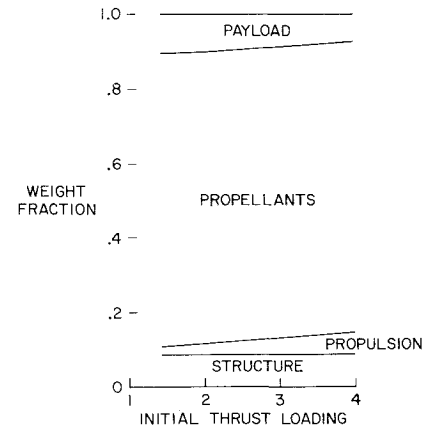

Fig. 18 Effect of second-stage thrust loading.

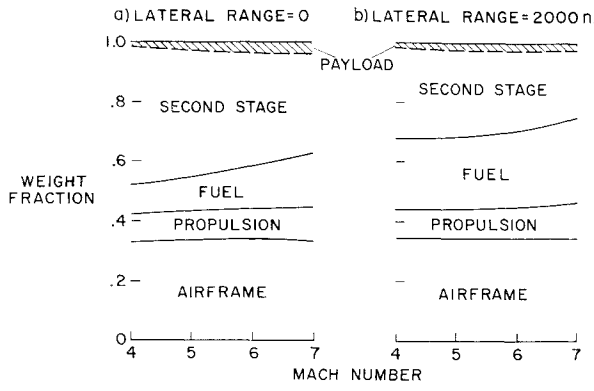

Fig. 19 Effect of design Mach number.

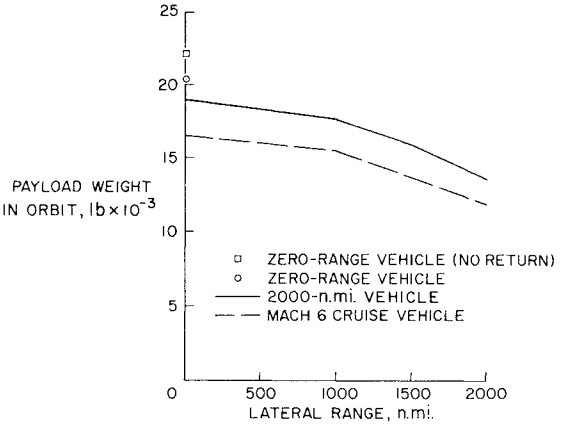

Fig. 20 Effect of lateral range requirement.

lateral range. All the vehicles in this comparison had a gross takeoff weight of 500,000 lb. The circled point at zero lateral range indicates a payload capability of about 20,000 lb for the vehicle that was designed with no lateral range requirement. (Actually, this zero-range vehicle could provide several hundred nautical miles of lateral range if it were not required to return to its takeoff point but instead was allowed to land at a convenient alternate field.) The square point above the circle represents the maximum zero-range capability of about 22,000 lb when the first stage contains no fuel after launch but is allowed to glide to a convenient landing field. The solid line represents the capability of a first stage designed to provide 2000 naut miles of lateral range. Second-stage sizes are varied with lateral range to provide maximum payload. If two properly sized second stages were used, this vehicle could orbit almost 19,000 lb at zero lateral range and about 13,500 lb at 2000-naut-miles lateral range. All the vehicles mentioned previously were designed for Mach number 7 operation, but nearly equal performance could be obtained with the Mach 6 vehicles.

The dotted line in Fig. 20 indicates the launch performance capability of the 500,000 lb, Mach 6 cruise vehicle which was studied previously.[3] As was mentioned, this aircraft can fly the study launch missions without difficulty, and in addition, it has sufficient fuselage volume to contain the necessary second stage. With a suitably modified fuselage, the cruise vehicle is capable of placing about 16,500 lb in orbit at zero lateral range; at 2000-naut-miles lateral range, its payload capability is about 12,000 lb.

The primary difference among the vehicles whose performance is shown in Fig. 20 is their fuselage volume which ranges from 42,000 ft^3 for the zero-range launch vehicle to 71,500 ft^3 for the cruise aircraft. In most other respects, the configurations are quite similar and the technologies required for their development appear to be virtually identical, with the exception, of course, of those technologies specifically related to the launch of the second stage.

Conclusions

The results of the present study indicate, once more, that a hydrogen-fueled, airbreathing, hypersonic aircraft can provide excellent performance when used as the first stage of an orbital launch system. For example, such an aircraft, grossing 500,000 lb, could take off from an airfield in the southern United States, cruise until it reached the vicinity of the equator, launch a second stage carrying a 13,000 lb, manned entry vehicle into an equatorial orbit, and return to its home base. The same aircraft, with a larger second stage, could orbit about 19,000 lb for a launch mission without the cruise requirement.

A comparison of the results of the present study with a previous study of hypersonic cruise vehicles indicates that both types of vehicles have similar characteristics. The primary difference between them is their fuselage volume; the cruise vehicles have considerably more volume than the launch vehicles. Although it appears desirable for the launch vehicles to have higher wing loadings than the cruise vehicles, takeoff and landing requirements tend to limit the wing loading of the launch vehicles to about the values used for cruise vehicles. Although high-speed maneuvers are required during the launch mission, optimum performance was obtained when these maneuvers were done at low load factors, and as a result, the structural and thermal problems appear no more severe for a launch mission than for a cruise mission. In fact, the study indicated that, with a fuselage modified to contain a second stage, the cruise vehicle would be capable of very respectable performance on a launch mission.

The quantitative results of the present study are based on rather restricted configurations and propulsion systems. Continued studies based on a broader range of configurations and engines, and on the results of continued aerodynamic, structural, and propulsion research, are necessary to determine the ultimate performance capabilities of turboramjet-powered, hypersonic aircraft. However, the present study does indicate that the technologies required for the development of both a cruise vehicle and a launch vehicle are practically identical; the only major difficulty uniquely associated with the launch mission is the possible problem of separating the two stages satisfactorily at launch. Finally, the study results suggest that a design Mach number of 6 is reasonable for aircraft powered by subsonic-burning turboramjets; higher design speeds increase the technology problems while offering only minor performance gains.

References

[1] Weber, R. J., "Propulsion for hypersonic transport aircraft," Fourth Congress International Council Aerospace Sciences, Preprint 64-558 (August 1964).

[2] Knip, G., Jr. and Allen, J. A., "Analysis of booster systems with a recoverable hypersonic airplane first stage," AIAA Preprint 64-543 (May 1964).

[3] Gregory, T. J., Petersen, R. H., and Wyss, J. A., "Performance trade-offs and research problems for hypersonic transports," J. Aircraft **2**, 266–271 (1965).

[4] Bergesen, A. J. and Porter, J. D., "An investigation of the flow around slender delta wings with leading edge separation," Princeton Univ., Dept. of Aeronautical Engineering, Rept. 510 (May 1960).

[5] Kelly, M. W., "Wind tunnel investigation of the low-speed aerodynamic characteristics of a hypersonic glider configuration," NACA RM A58F03 (1958).

[6] Koelle, H. H., *Handbook of Astronautical Engineering* (McGraw-Hill Book Co. Inc., New York, 1961).

[7] Ulmann, E. F. and Bertram, M. H., "Aerodynamic characteristics of low-aspect-ratio wings at high supersonic Mach numbers," NACA RM L53I23 (1953).

[8] Pitts, W. C., Nielsen, J. N., and Kaattari, G. E., "Lift and

center of pressure of wing-body-tail combinations at subsonic, transonic, and supersonic speeds," NACA TR 1307 (1957).

[9] Shanley, F. R., *Weight-Strength Analysis of Aircraft Structures* (Dover Publications Inc., New York, 1960), 2nd ed.

[10] Dickson, J. A., "Thermal protection with a temperature capability to 2500°F, for cool structures," *Proceedings of Conference on Aerodynamically Heated Structures*, edited by P. E. Glasser (Prentice-Hall, Englewood Cliffs, N. J., 1962), pp. 111–134.

[11] Fransiscus, L. C. and Lesberg, E. A., "Effects of nozzle recombination on hypersonic ramjet performance: II. Analytical investigation," AIAA J. 1, 2077–2083 (1963).

[12] Carlson, H. W., "The lower bound of attainable sonic-boom overpressure and design methods of approaching this limit," NASA TN D-1494 (1962).

[13] Hutchinson, H. A., "Defining the sonic boom problem," Astronaut. Aerospace Eng. 1 (December 1963).

[14] McLean, F. E., "Some nonasymptotic effects on the sonic boom of large airplanes," NASA TN D-2877 (1965).

[15] Bryson, A. E., Denham, W. F., Caroll, F. J., and Mikami, K., "Determination of lift or drag programs to minimize re-entry heating," J. Aerospace Sci. 29, 420–430 (1962).

[16] Stancil, R. T., "A new approach to steepest-ascent trajectory optimization," AIAA Preprint 63-223 (June 1963).

[17] *Specification for Engines, Aircraft, Turbojet, Model*, Military Specification MIL-E-5008B (January 1959).

SEPT.-OCT. J. AIRCRAFT VOL. 3, NO. 5

Some Experimental Contributions on Single Degree-of-Freedom Flutter in Two-Dimensional Low Supersonic Flow

YASUHARU NAKAMURA* AND YOSHIKAZU TANABE†
National Aerospace Laboratory, Chōhu, Tokyo, Japan

Two experimental investigations on the low supersonic instabilities were conducted in transonic wind tunnels. Firstly, the results are presented of the measurement of the unsteady pitching moment of a two-dimensional airfoil performing pitching oscillations in low supersonic flow. Secondly, a rotational motion of a flap has been investigated with a two-dimensional airfoil-flap combination model. A simple free oscillation method was adopted in the test in order to obtain the unsteady aerodynamic coefficients for oscillations at small amplitudes. Optical observations were made of the flowfield around the airfoil-flap combination model by using a highspeed cine camera for the case where the flap was hinged freely by ball bearings at both ends. In the first experiment, pure pitching instability of the airfoil was observed with the appropriate axis positions for all the values of Mach number and reduced frequency that were obtained. Rotational instability of the flap was observed also in the second experiment at every Mach number of the test. It is concluded from the results that the inviscid flow over the surfaces of the airfoil would be responsible primarily for the onset of these instabilities.

Nomenclature

I = moment of inertia of the system, kg-m-sec^2
$\bar{H}$ = unsteady aerodynamic hinge moment, $\bar{H} = \rho_\infty v_\infty^2 c_F^2 l(h_\beta \beta + c_F/v_\infty\, h_{\dot\beta}\dot\beta)$
$\bar{M}$ = unsteady aerodynamic pitching moment $\bar{M} = \rho_\infty v_\infty^2 c^2 l(m_\theta \theta + c/v_\infty\, m_{\dot\theta}\dot\theta)$
M_∞ = freestream Mach number
c = airfoil chord
c_F = flap chord
d = thickness of the metal strips used for cross spring pivots mm
f_0 = still air frequency of the system, cps
f = frequency of flap oscillation, cps
g_θ, g_β = structural damping of the system
h_β = aerodynamic stiffness coefficient of the unsteady hinge moment
$-h_{\dot\beta}$ = aerodynamic damping coefficient of the unsteady hinge moment
k = reduced frequency, $k = \omega c/2v_\infty$ or $\omega c_F/2v_\infty$
k_θ = torsional rigidity of the cross spring pivots, kg·m/rad
l = airfoil span
m_θ = aerodynamic stiffness coefficient of the unsteady pitching moment
$-m_{\dot\theta}$ = aerodynamic damping coefficient of the unsteady pitching moment
t = time
v_∞ = air velocity
x_0 = nondimensional distance along the chord from the leading edge
β = flap angle or its amplitude of oscillation
θ = pitching angle or its amplitude of oscillation
ρ_∞ = air density
ω = circular frequency, rad/sec
$\bar{\omega}$ = $2kM_\infty^2/(M_\infty^2 - 1)$
$\cdot$ = time derivative

Presented at the AIAA Symposium on Structural Dynamics and Aeroelasticity, Cambridge, Mass., August 30–September 1, 1965; submitted October 18, 1965; revision received March 14, 1966. The authors would like to express their cordial thanks to R. Kawamura and K. Washizu, of the University of Tokyo, for their instructive advice during the course of this study. They are also very grateful to N. C. Lambourne and H. C. Garner of the Aerodynamics Division, National Physical Laboratory, United Kingdom, who read the manuscript and offered valuable comments and criticism.

* Research Engineer, First Airframe Division.
† Research Engineer, First Airframe Division.

Introduction

ACCORDING to the linearized unsteady theory for two-dimensional transonic potential flow, the possibility of single degree-of-freedom flutter for a range of small values of reduced frequency is shown with both the pitching motion of an airfoil and with the rotational motion of a flap.[1–3]

However, there is a need for some experimental verification to support the foregoing theoretical statement since, in the